Supplemental material for: Global variability in radiative-convective equilibrium with a slab ocean under a wide range of CO_2 concentrations

Gabor Drotos[1,2,3]*, Tobias Becker[1], Thorsten Mauritsen[1,4], and Bjorn Stevens[1]

[1]*Max Planck Institute for Meteorology, Hamburg, Germany*
[2]*Instituto de Física Interdisciplinar y Sistemas Complejos (CSIC–UIB), Palma de Mallorca, Spain*
[3]*MTA–ELTE Theoretical Physics Research Group, Budapest, Hungary*
[4]*Meteorological Institute, Stockholm University, Stockholm, Sweden*
*Corresponding author. e-mail: `drotos@general.elte.hu` address: Carretera de Valldemossa, km 7,5 E-07122 Palma de Mallorca, Spain

S1 Visual inspection of spatial organization

Figure S1 illustrates in a particular time instant that regions of subsidence and ascendance, as identified by the vertical velocity ω (in pressure coordinates) at model level 41 (ω_{41}, see Section 4.1 for why it is used), are finely intertwined in the control run ($n = 1$), while they form two separate aggregated blobs for 16-fold CO_2 concentration ($n = 4$).

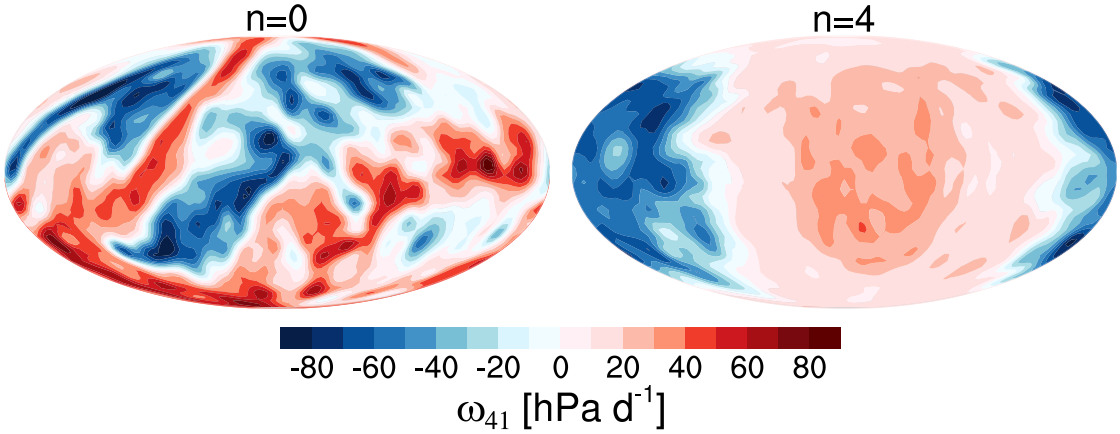

Figure S1: Snapshots of the vertical velocity ω (in pressure coordinates) at model level 41 (ω_{41}) at $t = 2727$ (cf. Fig. 6) in two runs with different CO_2 concentration as indicated in the panels by n of Equation (1) of the main text.

S2 Spatial variation of the cloud-layer stability and why the dry-subsiding region is studied

Fig. S2 illustrates, in different phases of a cooling event, the spatial variation of the cloud-layer stability $\Delta\theta_{\mathrm{CLS}}$, most relevant for the formation of the stratiform clouds, in terms of the ascendance or subsidence strength ω_{41} defined at model level 41. It becomes clear that two regions of very different character exist in any phase.

One of the regions can be identified in the plots as a group of points aligned along a nearly horizontal line that starts in the ascending region ($\omega_{41} < 0$) and extends well into the region of subsidence ($\omega_{41} > 0$), and remains mostly invariant during the cooling event. This region is the one that hosts deep convection, but can be treated as a single block from the point of view of stratiform cloud formation (in particular, no stratiform clouds can form here).

The other region appears as a blob in the region of subsidence ($\omega_{41} > 0$), off the line described previously. It is approximately captured by an empirical dryness condition, $q < \frac{2}{3}\mathrm{max}_{\mathrm{spatial}}(q)$ at level 41, beyond masking for $\omega_{41} > 0$, as the highlighting by gray background in Fig. S2 shows — this is what we call the 'dry-subsiding' region.

As long as shallow convection is penetrative in the dry-subsiding region (Fig. S2a), this region is more *unstable* in terms of the cloud-layer stability $\Delta\theta_{\mathrm{CLS}}$ than the main

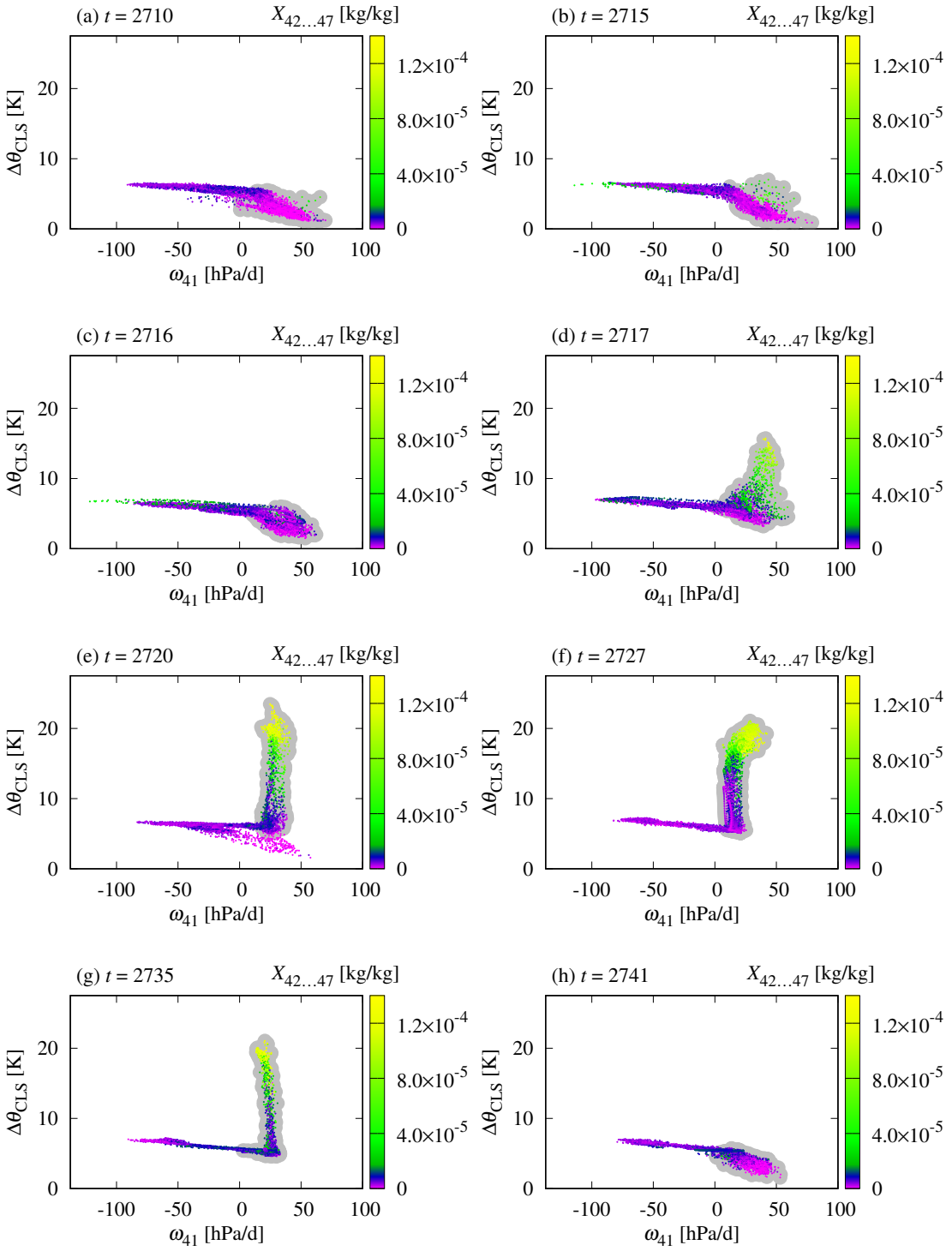

Figure S2: The cloud-layer stability $\Delta\theta_{\mathrm{CLS}} = \theta(\mathrm{level41}) - \theta(\mathrm{level44})$ (as defined in Section 4) as a function of the vertical velocity ω_{41} (in pressure coordinates, see Sections 3.1 and 4) for different geographical positions at the indicated time instants (corresponding to those of Figs. 6 and 7 with two additional ones). Each point in the plots corresponds to a grid point on the sphere. Background shading in gray marks grid points that fulfill $\omega_{41} > 0$ and $q < \frac{2}{3}\mathrm{max}_{\mathrm{spatial}}(q)$ at model level 41 (see text and Section 4). Coloring represents the cloud liquid water content X averaged for levels 42 to 47.

convection-hosting region. The dry-subsiding region hosts even *less* clouds at low atmospheric levels, see the coloring in Fig. S2a. However, after penetrative shallow convection shuts down (which starts in Fig. S2b, with a momentary stop in Fig. S2c, but then extends to Figs. S2e-S2g), $\Delta\theta_{\mathrm{CLS}}$ extends to very high values. As the coloring $X_{42...47}$ in Figs. S2b-S2g suggests, the higher $\Delta\theta_{\mathrm{CLS}}$ is, the more low-level clouds are found there. After shallow convection becomes penetrative again in the dry-subsiding region (Fig. S2h), the configuration of the investigated quantities returns to its initial state (i.e., Fig. S2a).

Since the dry-subsiding region has well-defined distinguishing characteristics during the whole cycle of the cooling event, and low-level (stratiform) clouds, according to the coloring in Figs. S2b-S2g, fill almost the entire region but not more, it seems to be reasonable to concentrate on the dry-subsiding region in our analyses.

S3 Spatial variation of $\Delta q_{41,44}$ in the dry-subsiding region

Figure S3 illustrates how the spatial variation of the difference $\Delta q_{41,44}$ in the specific humidity (introduced in Section 4 to characterize how strong shallow convection is in the dry-subsiding region) is related to that of the lower tropospheric stability $\Delta\theta_{\mathrm{LTS}}$, in different phases of a cooling event. We concentrate on the dry-subsiding region, but, for completeness, we plot in peach all other grid points of the sphere, too.

Before the cooling event begins (Fig. S3a), $\Delta\theta_{\mathrm{LTS}}$ is smaller than 20 K, and $\Delta q_{41,44}$ is dominantly greater than -0.005 in the dry-subsiding region. The formation of the stratiform cloud field (see the coloring) comes along in a separate branch of points with increased values of $\Delta\theta_{\mathrm{LTS}}$, accompanied by a decreasing tendency in $\Delta q_{41,44}$, see Fig. S3b. Although the first cloud field is not permanent, see the coloring in Fig. S3c, the process continues from Fig. S3d. As the cooling event develops more, shown in Fig. S3e, much higher values of $\Delta\theta_{\mathrm{LTS}}$ and much lower values of $\Delta q_{41,44}$ are reached. There is a clear anticorrelation between the two variables outside the cloud field. However, where clouds are most abundant and the lower troposphere is most stable, $\Delta q_{41,44}$ is again higher. This remains so during the later evolution of the cooling event as well (Figs. S3f-S3g). When the stratiform cloud field desiccates (Fig. S3h, see the coloring), the lowest values of $\Delta q_{41,44}$ disappear; in particular, $\Delta q_{41,44}$ becomes rather uniformly distributed in the range of its initial values (those in Fig. S3a). $\Delta\theta_{\mathrm{LTS}}$, however, needs more time to relax (see the discussion in Section 4).

What we learn from Fig. S3 is that the lower tropospheric stability $\Delta\theta_{\mathrm{LTS}}$ and the proxy $\Delta q_{41,44}$ for the strength of the shallow convection are strongly related even locally at the beginning of the cooling event, and that the desiccation of the cloud field happens when the values of $\Delta q_{41,44}$ return to their initial range, i.e., the range before the beginning of the cooling event. All of this is so in spite of the fact that $\Delta q_{41,44}$ behaves nontrivially within the cloud field during the bulk of the cooling event.

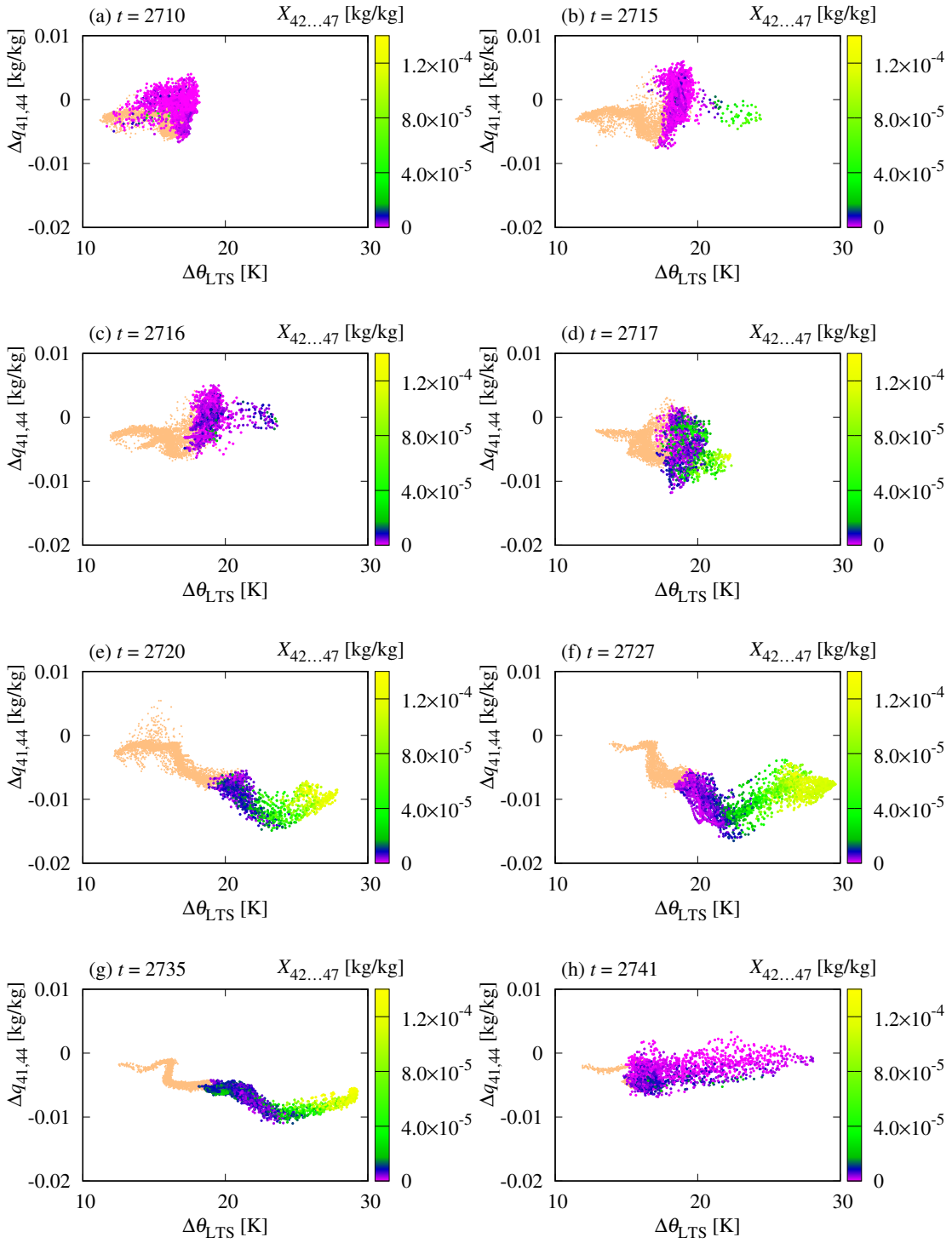

Figure S3: The difference $\Delta q_{41,44}$ in the specific humidity (see Section 4) as a function of the lower tropospheric stability $\Delta\theta_{\mathrm{LTS}}$ (as defined in the same section) for different geographical positions at the indicated time instants (corresponding to those of Figs. 6 and 7 with two additional ones). Each point in the plots corresponds to a grid point on the sphere. The points with a color from the color scale are in the dry-subsiding region (see Sections 4 and S2), and coloring represents the cloud liquid water content X averaged for levels 42 to 47. The points in peach are located in the rest of the globe.

S4 Formation of a new ascending region

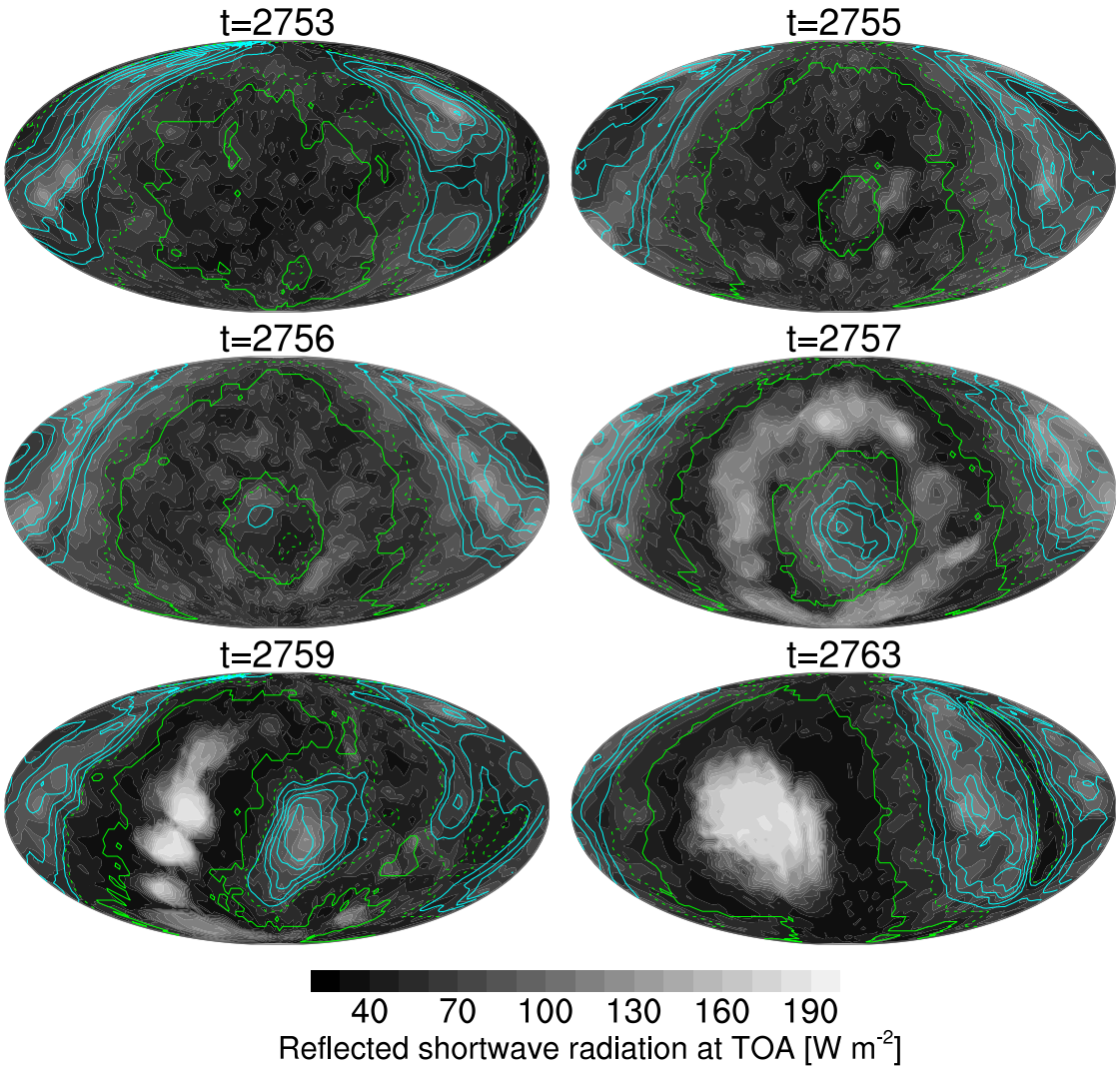

Figure S4: Same as Fig. 6, but for other time instants.

Figure S4 is the continuation of the series of snapshots that starts in Fig. 6. According to Fig. S4, during the warming phase, near $t = 2755$, a new ascending region forms in the middle of the subsiding region, where the stratiform cloud field used to be during the earlier cooling event presented in Fig. 6. The emergence of the new ascending region is soon accompanied by the appearance of a new stratiform cloud field in the remaining part of the dry-subsiding region, which has the shape of a ring, see $t = 2757$ in Fig. S4. Around $t = 2579$, the new ascending region is expelled from the ring-shaped subsidence region, and finally merges with the already existing one ($t = 2763$). This is how the original, bipolar spatial structure is recovered, which was broken by the appearance of the new ascending region.

Although the last major event before that of Fig. S4 is the one presented in Fig. 6, a similar event, but with much smaller scales, also occurs in between.

S5 Phase space analysis: extension to $\Delta q_{41,44}$

In this section, we extend the phase space analysis presented in Section 4.2 of the main text to illustrate the importance of the strength of the shallow convection in the dry-subsiding region via the moisture-based proxy $\Delta q_{41,44}$.

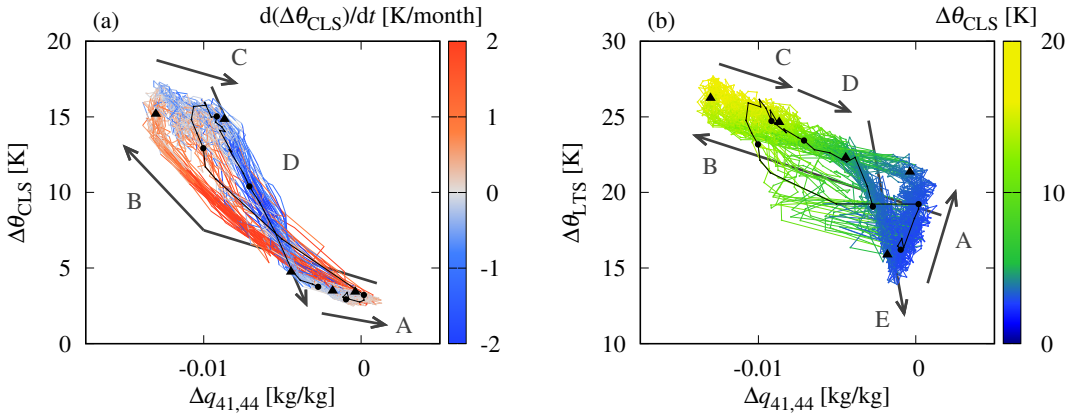

Figure S5: Phase space projections for quantities in the dry-subsiding region: (a) the spatial mean of $\Delta q_{41,44}$ and that of $\Delta\theta_{\mathrm{CLS}}$, with coloring corresponding to the discrete time derivative, calculated from the consecutive time steps, of the latter spatial mean, and (b) the spatial mean of the lower tropospheric stability $\Delta\theta_{\mathrm{LTS}}$, of $\Delta q_{41,44}$, and of $\Delta\theta_{\mathrm{CLS}}$. Additional features are as in Fig. 10 of the main text. $n = 4$.

Figure S5a suggests that $\Delta\theta_{\mathrm{CLS}}$ is strongly related to the strength of the penetrative shallow convection, expressed in terms of $\Delta q_{41,44}$. In particular, as $\Delta q_{41,44}$ decreases, $\Delta\theta_{\mathrm{CLS}}$ increases (section B). During the capped phase (section C), the tendencies become opposite: $\Delta q_{41,44}$ increases, and $\Delta\theta_{\mathrm{CLS}}$ decereases, but only slightly. A substantial weakening of stability at the cloud layer is identified by section D (as highlighted by the coloring), when $\Delta\theta_{\mathrm{CLS}}$ substantially reduces. The main re-establishment of ventilating shallow convection is in this phase.

The path through the phase space defined by $\Delta\theta_{\mathrm{LTS}}$ instead of $\Delta\theta_{\mathrm{CLS}}$ shows many similarities, see Fig. S5b. A major difference is an increase of $\Delta\theta_{\mathrm{LTS}}$ in section A. As also indicated in the main text, we hypothesize that this process is what leads to the attenuation of shallow convection to finally prevent it from penetrating the layer where stratiform clouds form subsequently. Note that $\Delta\theta_{\mathrm{CLS}}$ is not increasing at all in section A (see Fig. S5a), so that we cannot explain the shutdown of penetration in terms of $\Delta\theta_{\mathrm{CLS}}$. While the shutdown point in $\Delta\theta_{\mathrm{LTS}}$ is not unique, in Fig. S5b we can clearly identify two bunches of trajectories entering to section B, near $\Delta\theta_{\mathrm{LTS}} = 18\,\mathrm{K}$ and 22 K. Trajectories of the former bunch, like the one highlighted in black, enter then earlier into section C, i.e., the cycle is smaller.

The other major difference between $\Delta\theta_{\mathrm{LTS}}$ and $\Delta\theta_{\mathrm{CLS}}$ is a lag of the former in sections of the cycle other than A, compare Figs. S5b and S5a. The most informative manifestation of this lag is a substantial reduction in $\Delta\theta_{\mathrm{LTS}}$ in section E, in association with the rise of surface temperatures subsequent to the desiccation of the stratiform cloud layer. $\Delta\theta_{\mathrm{CLS}}$ remaining constant in section E but decreasing earlier (in section D) confirms that the stratification in the lower layers, in spite of $\Delta\theta_{\mathrm{LTS}}$

not yet having relaxed, is already set during section E by the shallow convection which now penetrates through the layer where the stratiform clouds used to be, to ventilate the lower troposphere.

S6 Some properties of the cycle in the lower mid-troposphere

In Section 4.2, gravity waves originating from the deep convection taking place in the region of ascendance are supposed to set the temperature of the lower mid-troposphere in the dry-subsiding region during most of the ventilated phase. Gravity waves act to level the isopycnals and thereby to homogenize the virtual potential temperature (e.g. Bretherton and Smolarkiewicz, 1989; Sobel and Bretherton, 2000). To test whether the idea can hold, we investigate here the difference of the spatially averaged virtual potential temperature at 700 hPa between the two regions. In particular, we plot this difference on the vertical axis in a phase space representation that is otherwise the same as in Fig. 10a.

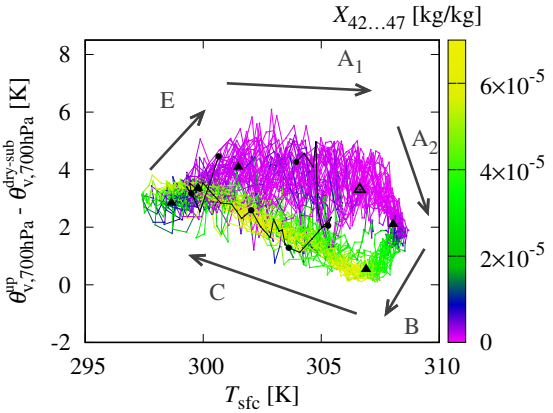

Figure S6: Phase space projection: the spatial mean of the surface temperature T_{sfc} in the dry-subsiding region, the difference of the spatially averaged virtual potential temperature at 700 hPa between the ascending and dry-subsiding regions, and the spatial mean of the cloud liquid water content $X_{42...47}$ in the dry-subsiding region. Additional features are marked as in Fig. 10. Furthermore, an empty triangle is displayed between the two subsections of section A, corresponding to $t = 2809$.

According to Fig. S6, this difference is practically constant (with considerable fluctuations) during the bulk of the ventilated phase, labeled as section A_1. This confirms that the temperatures of the lower mid-troposphere of the two regions are very closely related, so that the assumption of Section 4.2 may hold indeed. Note, however, that the difference is not zero, which suggests that some other factors may also be involved in determining the 700 hPa virtual potential temperature in the dry-subsiding region: in particular, some additional cooling effects may be present.

In the subphase labeled as A_2, cf. Fig. 10b, some rearrangement takes place. Since there is no cooling yet in the region of ascendance (see Fig. 8), this must be a warming of the lower mid-troposphere in the dry-subsiding region. As discussed in Section 4.2, shallow convection in the dry-subsiding region is already beginning

to lose its penetrative power in this subphase: in particular, it does not reach as high to the atmosphere as before. As a consequence, cooling from evaporation and the strong moisture gradient becomes absent at 700 hPa, and this is what results in warming. In view of this process, it seems plausible that the lower mid-troposphere was kept colder by the mentioned cooling factors in the previous subsection, A_1.

In section B, surface cooling in the dry-subsiding region also begins besides further warming in the lower mid-troposphere; the latter is due to shallow convection still getting weaker, cf. Fig. S5. By section C, the surface cooling gets communicated to the ascending region, which results in cooling of the free troposphere globally (with the mediation of deep convection). Shallow convection in the dry-subsiding region is gaining strength from this point on (see again Fig. S5), and, as a result of the associated cooling effects, the difference in the virtual potential temperature in Fig. S6 also starts increasing. After a momentary stop in section D (not labeled in Fig. S6), this difference is finally raised to its initial value in section E: by the time when section A begins next, the shallow convection and the associated cooling effects reach their full power.